学术期刊可以用微信做什么，快来看看！

可全面技术输出

微信自动应答服务平台

微时代 微革命

微服务

移动互联网时代的营销革命

简单快捷 · 高效互动 · 随时随地 · 广泛传播

微信扫一扫

开启智慧“微服务”

Highly efficient narrow-band plasmonic waveguide filter based on cascaded slot cavities

Zongqiang Chen (陈宗强), Jing Chen (陈 靖), Yudong Li (李玉栋), Jun Qian (钱 郡), Jiwei Qi (齐继伟), Jingjun Xu (许京军), and Qian Sun (孙 骞)*

MOE Key Laboratory of Weak Light Nonlinear Photonics, Tianjin Key Laboratory of Photonics Material and Technology, School of Physics, Nankai University, Tianjin 300071, China

**Corresponding author: qiansun@nankai.edu.cn*

Received April 3, 2013; accepted September 16, 2013; posted online November 4, 2013

A novel plasmonic waveguide filter design based on three cascaded slot cavities is proposed. The cascaded nanocavities support a united resonant (UR) mode. Light is trapped in the middle nanocavity at telecommunication wavelength (1550 nm) when the UR mode exists. This phenomenon leads to the efficient transmittance and high Q factor of the plasmonic filter. The resonant wavelength and Q factor can be easily modulated by the cavity radii and the waveguide width.

OCIS codes: 240.6680, 230.7408, 130.3120.
doi: 10.3788/COL201311.112401.

Surface plasmon polaritons (SPPs) are evanescent waves propagating along the interface between a metal and a dielectric, thus providing great potential to overcome the diffraction limit of light[1−3]. Metal-insulator-metal (MIM) waveguides are examples of typical devices based on SPPs that confine light in subwavelength dimensions. Numerous plasmonic devices, which are based on the MIM structure, have been demonstrated; these devices include beam splitters[4,5], wavelength demultiplexers[6,7], logic gates[8], all-optical switches[9], Mach-Zennder interferometers[10], and networks[11].

Many studies have recently focused on MIM plasmonic filters. An optical cavity with a high Q factor is a key component of plasmonic filters. Cavities can be classified into two types according to the ways they couple light. The first type of cavity is called coupled cavity, which is separated from the MIM waveguide, i.e., a gap exists between the cavity and the waveguide. Coupled cavities such as ring resonators[12], nanodisk resonators[13], slot cavities[14], and rectangular ring resonators[15−18] have been demonstrated as band-pass or band-stop filters. The drawback of coupled cavities is their low transmittance, which results from reflection and internal losses caused by the metal partition between the waveguide and the cavity. For example, when the gap between a coupled cavity and waveguide is 10 nm, the plasmonic filter transmittance is approximately 60%[12−18]. As the gap increases, the transmittance drops sharply. The second type of cavity is called connected cavity[19,20], which connects directly to the waveguide, i.e., no gap exists between the cavity and the waveguide. Direct connection between the cavity and the waveguide guarantees high device transmittance. However, the power in such a cavity escapes to the MIM waveguide fairly easily, which decreases the Q factor. For example, when a connected cavity is integrated with an MIM waveguide[19,20], the Q factor is only approximately 2, much less than the Q factor (about several tens) of coupled cavities.

Previous studies focused on MIM waveguide interactions with single cavities, and the interaction between cavities has received little attention. In the current study, a narrow-band plasmonic filter based on three connected cascade slot cavities is studied. The cascaded slot cavities interact with each other and generate a new resonant mode. Our design features a high Q factor, which is attributed to high energy congregation in the cascaded slot cavities, and high transmittance, which is due to the direct connection between the cavity and the MIM waveguide.

No analytical solution of the resonant mode of cascaded slot cavities has yet been published. In this letter, the eigenmodes of cascaded cavities are analyzed via the finite-element analysis method (FEM) using commercial software (COMSOL Multiphysics). Figure 1(a) shows the geometry of a single circular nanocavity. The junction between circumscribed nanocavities contains a MIM waveguide with D=50 nm (Fig. 1(b)). The configuration yields a convergence result because of our avoidance of sharp metal corners. The insulator in the cavity is air (n_d=1), and the metal is silver, the frequency-dependent complex relative permittivity of which is characterized by the Drude model:

$$\varepsilon_{\mathrm{m}}(\omega) = \varepsilon_{\infty} - \omega_{\mathrm{p}}^2/\omega(\omega + \mathrm{i}\gamma), \tag{1}$$

where ε_{∞} is the dielectric constant at the infinite frequency, γ is the electron collision frequency, ω_{p} is the bulk plasma frequency, and ω is the angular frequency of incident light. The parameters are ε_{∞}=3.7, ω_{p}=9.1 eV, and γ=0.018 eV[21].

Figures 1(c)–(e) show the magnetic field $|\mathbf{H}_z|$ amplitude distribution of different configurations of cascaded disk-shaped cavities. Figure 1(c) displays the distribution $|\mathbf{H}_z|$ of the eigenmode in two cascaded disk-shaped cavities, thereby revealing the equipartition density of the magnetic field. In two unequal cascaded disk-shaped cavities, the density of the magnetic field in the smaller disk-shaped cavity is greater than that in the larger one, which is shown in Fig. 1(d). For further enhancement of the magnetic field in the small disk-shaped cavity, three cascaded disk-shaped cavities are considered as a candidate configuration. The eigenmode of the three cascaded

cavities is presented in Fig. 1(e). In FEM, the complex-valued eigenfrequency is $f = f_{\rm re} + {\rm i}f_{\rm im}, Q_{\rm cd} = f_{\rm re}/2f_{\rm im}$. The calculated Q factor consists of contributions from intrinsic metal losses $Q_{\rm metal}$ and geometry- and material-dependent radiation losses $Q_{\rm rad}$ into free space[22]:

$$Q_{\rm cd}^{-1} = Q_{\rm metal}^{-1} + Q_{\rm rad}^{-1}. \quad (2)$$

The Q factors of the cavities in Figs. 1(c)–(e) are 144, 173, and 337, respectively. The cascaded circular nanocavities produce a new resonant mode, which is called the united resonant (UR) mode.

Figure 2 shows the geometry of the two-dimensional plasmonic filter, which is composed of an MIM waveguide and three cascaded disk-shaped cavities. Three circumscribed cavities are embedded into an MIM waveguide. The cavity centers are kept in the center line of the MIM waveguide to preserve structural symmetry along the x- and y-axes. The radii of the bilateral disk-shaped cavities are the same and denoted as R_1. Furthermore, the radius of the middle disk-shaped cavities is denoted as R_2, and the waveguide width is D. The input light is a transverse magnetic (TM) plane wave that excites the SPPs.

Figure 3(a) depicts the plasmonic filter transmittance calculated by FEM. The transmittance is defined as $T = |\mathbf{H}_{\rm zout}|^2/|\mathbf{H}_{\rm zin}|^2$, where $|\mathbf{H}_{\rm zin}|$ and $|\mathbf{H}_{\rm zout}|$ are the input

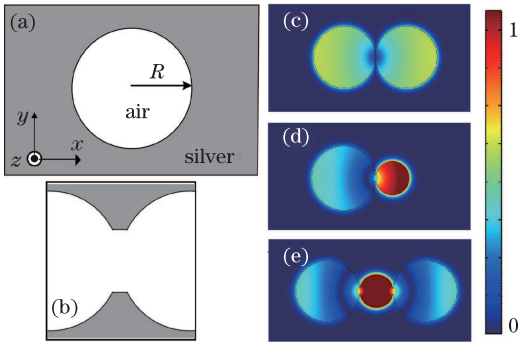

Fig. 1. (Color online) (a) A single disk-shaped cavity. (b) Schematic diagram of the junction between the cascaded cavities. For visualization, the diagram is not shown in true proportions. The distribution $|\mathbf{H}_z|$ of the eigenmode: (c) two equal cascaded cavities, (d) two unequal cascaded cavities, and (e) three cascaded cavities (two big cavities and a small cavity). The wavelengths of the resonance modes in (c), (d), and (e) are 3300, 2160, and 1550 nm, respectively. Here, the radius of large cavities is 260 nm while that of the small cavities is 135 nm.

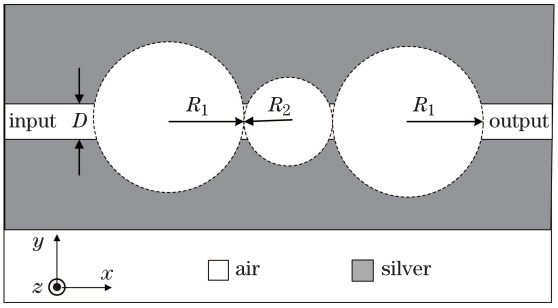

Fig. 2. Schematic diagram of the proposed plasmonic filter.

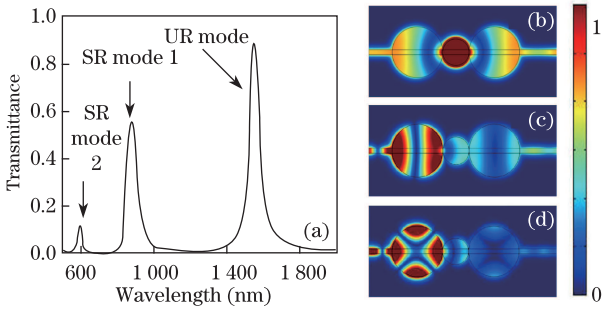

Fig. 3. (Color online) (a) Transmission spectrum of the plasmonic filter based on three cascaded cavities. Here, R_1=260 nm, R_2=135 nm, and D=50 nm. The $|\mathbf{H}_z|$ field distributions at three transmission peaks with wavelengths of 1550, 880, and 595 nm are shown in (b), (c), and (d), respectively.

and output amplitudes, respectively, of the magnetic field. The parameters of the filter structure are set as R_1= 260 nm, R_2= 135 nm, and D= 50 nm. Three transmission peaks corresponding to wavelengths λ of 1550, 880, and 595 nm are observed. Field distributions of $|\mathbf{H}_z|$ at incident λ of 1550, 880, and 595 nm are depicted in Figs. 3(b)–(d), respectively, and the resonant mode transmittances at these wavelengths are 90%, 55%, and 12%, respectively.

In our filter, two types of resonant modes exist, i.e., the UR mode and the single-disk resonant (SR) mode. The UR mode corresponds to Fig. 3(b) and originates from the eigenmode of three cascaded disk-shaped cavities (Fig. 1(e)). Interestingly, the light is highly localized in the middle cavities. In FEM, the input light magnitude is 1 A/m. The average value of the magnetic field in the middle cavity is 3.5 A/m. Since energy density $I \propto |H|^2$, the energy density in the middle cavities increases by approximately 10-fold. Therefore, the UR mode produces a high Q factor. This new resonant mode of the UR system has a fairly high transmittance (about 90%) and can be tuned to the telecommunication wavelength (1550 nm). To the best of our knowledge, the UR mode has never been explicitly studied in previous research.

The resonance can also be excited in disk-shaped cavities, i.e., the SR modes in Fig. 3. The SR mode in bilateral disk-shaped cavities satisfies the resonant condition, which is given by[13]

$$k_{\rm d}\frac{H_n^{(1)'}(k_{\rm m}r)}{H_n^{(1)}(k_{\rm m}r)} = k_{\rm m}\frac{J_n'(k_{\rm d}r)}{J_n(k_{\rm d}r)}, \quad (3)$$

where $k_{\rm d,m}$ are the wave vectors in the dielectric disk/metal; r is the radius of the nanocavity; J_n and J_n' are the first-kind Bessel functions with the order n and its derivation, respectively; $H_n^{(1)}$ and $H_n^{(1)'}$ are first-order Hankel functions with the order n and its derivation, respectively. The SR mode transmittances, which correspond to Figs. 3(c) and (d), are lower than those of the UR mode. This phenomenon is attributed to the mismatch between resonant wavelengths ($\lambda_{\rm r}$) in the middle disk-shaped cavities and $\lambda_{\rm r}$ in adjacent cavities in the SR mode.

To further investigate the UR mode properties of the

filter, the Q factor of the filter is estimated by[23]

$$Q_{\mathrm{f}} = \frac{\lambda_{\mathrm{r}}}{\mathrm{FWHM}}, \tag{4}$$

where λ_{r} is the resonant wavelength and FWHM is the full-width at half-maximum of the UR mode transmission spectra. When the device parameters are R_1=260 nm, R_2=135 nm, and D=50 nm, the UR mode FWHM is 55 nm. The Q factor of the UR mode, which is estimated by Eq. (4), is 28. This Q_{f} may be improved significantly when compared with the theoretical value (337) of cascaded disk-shaped cavities. The decrease in Q factor is attributed to radiation losses Q_{rad} into the MIM waveguide. Figure 4 depicts the dependence of Q_{f} on R_1/D. When the R_1/D value increases, i.e., R_1=260 nm, R_2=135 nm, and D=25 nm, Q_{f} can reach 56. For Q_{f}, the higher the increase in R_1/D value, the smaller the relative connected area between the cavities and the MIM waveguide. Thus, more energy is stored in the cavity and less power is dissipated from the cavity.

Figure 5 displays the influence of the device parameters on the λ_{r} of the UR mode. Figure 5(a) shows the transmission spectra obtained under different R_2 when R_1 and D are maintained at 260 and 50 nm, respectively. Figures 5(b) and (c) show the dependence of the λ_{r} on R_2 and R_1. The results reveal that λ_{r} depends on R_2 (R_1) in a linear manner, which is consistent with the case of a normal cavity. The slope of the linear dependence of λ_{r} on R_2 is 8.6, i.e., when the radius of the middle disk-shaped cavity R_2 increases by 1 nm, the λ_{r} has a red shift of 8.6 nm. The slope of the linear dependence of λ_{r} on R_1 is 1.8, which is smaller than that observed in the case of R_2. The middle disk-shaped cavity has a larger impact on transmission response of the UR mode than the adjacent cavities, which is likely due to high energy congregation in the middle disk-shaped cavity. Figure 5(d) shows that λ_{r} decreases as the D increase. The junction of the adjacent disk-shaped cavities is a MIM waveguide. When D increases, the effective refractive index of the MIM waveguide decreases[21]. This process causes a blue shift in the λ_{r}.

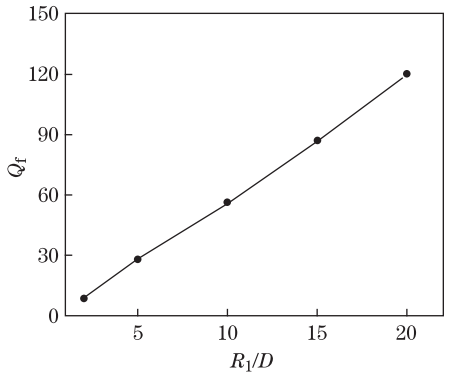

Fig. 4. Dependence of Q_{f} on R_1/D under a fixed R_1=260 nm and R_2=135 nm.

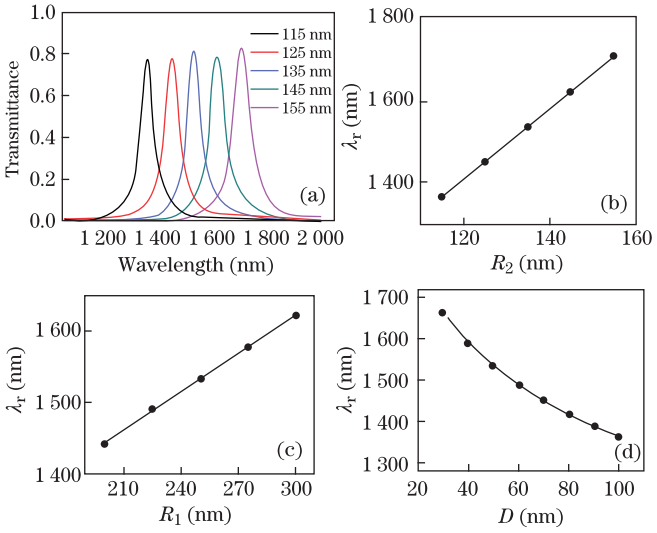

Fig. 5. (Color online) Influence of filter parameters on the UR mode. (a) Transmission spectra with different R_2 when R_1=260 nm and D=50 nm. The resonant wavelength λ_{r} versus R_2 (b) when R_1=260 nm and D=50 nm, versus R_1 (c) when R_2=135 nm and D=50 nm, and versus D (d) when R_1=260 nm and R_2=135 nm.

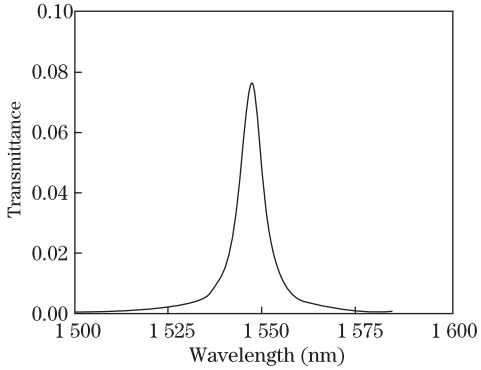

Fig. 6. Transmission spectrum of the plasmonic filter based on three cascaded disk-shaped cavities when a 10-nm gap is found between the MIM waveguide and the cavity.

Finally, the configuration where a gap exists between the resonator and the MIM waveguide is illustrated. Figure 6 shows the transmission spectrum of the plasmonic filter based on three cascaded disk-shaped cavities when a 10-nm gap is found between the resonator and the MIM waveguide. The transmittance of this configuration is 8%, much lower than that of our proposed structure. The gap between the resonator and the MIM waveguide leads to more energy stored in the cavity and less power dissipated from the cavity; thus, the Q factor of this configuration is approximately 260, much higher than that of our proposed structure.

In conclusion, a novel narrow-band plasmonic waveguide filter design based on cascaded slot cavities is proposed and numerically demonstrated by FEM. The cascaded slot cavities support a UR mode, which originates from coupling among the slot cavities. The UR mode presents a high Q factor and efficient transmittance at telecommunication wavelength (1550 nm). The λ_{r} and Q factor can be easily modulated by the slot cavity radii and the MIM D. Our findings indicate that cascaded cavities are interesting candidate materials for high-density nanophotonic integrated circuits.

This work was supported by the National Natural Science Foundation of China (No. 61178004), the Research Fund for the Doctoral Program of Higher Education of China (No. 20110031120005), Tianjin Natural

Science Foundation (Nos. 12JCQNJC01100 and 13JCQNJC01700), and the Program for Changjiang Scholars and Innovative Research Team in Nankai University.

References

1. W. Barnes, A. Dereux, and T. Ebbesen, Nature **424,** 824 (2003).
2. X. Wang, P. Wang, C. Chen, J. Chen, Y. Lu, H, Ming, and Q. Zhan, Chin. Opt. Lett. **8,** 584 (2010).
3. X. Li, Q. Tan, B. Bai, and G. Jin, Chin. Opt. Lett. **10,** 052401 (2012).
4. G. Veronis and S. Fan, Appl. Phys. Lett. **87,** 131102 (2005).
5. J. Chen, Z. Li, M. Lei, X. Fu, J. Xiao, and Q. Gong, Plasmonics **7,** 441 (2012).
6. G. Wang, H. Lu, X. Liu, D. Mao, and L. Duan, Opt. Express **19,** 3513 (2011).
7. F. Hu, H. Yi, and Z. Zhou, Opt. Lett. **36,** 1500 (2011).
8. Z. Chen, J. Chen, Y. Li, D. Pan, W. Lu, J. Xu, and Q. Sun, IEEE Photon. Technol. Lett. **24,** 1366 (2012).
9. A. A. Reiserer, J. Huang, B. Hecht, and T. Brixner, Opt. Express **18,** 11810 (2010).
10. B. Wang and G. Wang, Opt. Lett. **29,** 1992 (2004).
11. E. Feigenbaum and H. A. Atwater, Phys. Rev. Lett. **104,** 147402-1 (2010).
12. T. Wang, X. Wen, C. Yin, and H. Wang, Opt. Express **17,** 24096 (2009).
13. H. Lu, X. Liu, D. Mao, L. Wang, and Y. Gong, Opt. Express **18,** 17922 (2010).
14. F. Hu, H. Yi, and Z. Zhou, Opt. Express **19,** 4848 (2011).
15. A. Hosseini and Y. Massoud, Appl. Phys. Lett. **90,** 181102 (2007).
16. B. Yun, G. Hu, and Y. Cui, J. Phys. D: Appl. Phys. **43,** 385102 (2010).
17. J. Liu, G. Fang, H. Zhao, Y. Zhang, and S. Liu, J. Phys. D: Appl. Phys. **43,** 055103 (2010).
18. I. Zand, A. Mahigir, T. Pakizeh, and M. S. Abrishamian, Opt. Express **20,** 7516 (2012).
19. X. Lin and X. Huang, Opt. Lett. **33,** 2874 (2008).
20. Y. Matsuzaki, T. Okamoto, M. Haraguchi, M. Fukui, and M. Nakagaki, Opt. Express **16,** 16314 (2008).
21. Z. Han, E. Forsberg, and S. He, IEEE Photon. Technol. Lett. **19,** 91 (2007).
22. B. Min, E. Ostby, V. Sorger, E. Ulin-Avila, L. Yang, X. Zhang, and K. Vahala, Nature **457,** 455 (2009).
23. X. Serey, S. Mandal, and D. Erickson, Nanotechnology **21,** 305202 (2010).